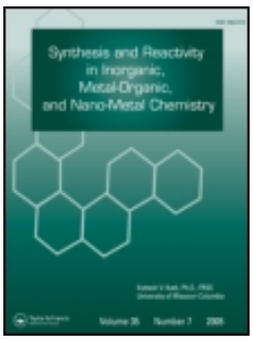

Synthesis and Reactivity in Inorganic, Metal-Organic, and Nano-Metal Chemistry

ISSN: 1553-3174 (Print) 1553-3182 (Online) Journal homepage: https://www.tandfonline.com/loi/lsrt20

Fabrication of Nanoporous Alumina and Their Structural Characteristics Study Using SEM Image Processing and Analysis

K. S. Choudhari , P. Jidesh & N. K. Udayashankar

To cite this article: K. S. Choudhari , P. Jidesh & N. K. Udayashankar (2012) Fabrication of Nanoporous Alumina and Their Structural Characteristics Study Using SEM Image Processing and Analysis, Synthesis and Reactivity in Inorganic, Metal-Organic, and Nano-Metal Chemistry, 42:3, 369-375, DOI: 10.1080/15533174.2011.611206

To link to this article: https://doi.org/10.1080/15533174.2011.611206

Synthesis and Reactivity in Inorganic, Metal-Organic, and Nano-Metal Chemistry, 42:369–375, 2012

ISSN: 1553-3174 print / 1553-3182 online
DOI: 10.1080/15533174.2011.611206

Taylor & Francis
Taylor & Francis Group

Fabrication of Nanoporous Alumina and Their Structural Characteristics Study Using SEM Image Processing and Analysis

K. S. Choudhari,[1] P. Jidesh,[2] and N. K. Udayashankar[1]

[1]*Department of Physics, National Institute of Technology Karnataka, Srinivasnagar, Surathkal, India*
[2]*Department of Mathematical and Computational Sciences, National Institute of Technology Karnataka, Srinivasnagar, Surathkal, India*

Nanoporous anodic aluminum oxide (AAO) membranes were fabricated by a two-step anodization process. Quantitative structural characterization was carried out using scanning electron microscopy images of the fabricated anodized alumina. An algorithm based on mathematical morphology was developed to extract pore size distribution with average, minimum, and maximum pore diameter of the nanoporous alumina. This technique of obtaining quantitative data based on image analysis could be an efficient, unbiased, and reliable method and can be used to control the fabrication parameters of anodization process.

Keywords anodic aluminum oxide, anodization, mathematical morphology analysis, scanning electron microscopy

INTRODUCTION

In recent years there has been tremendous growth in the field of nanoscience and nanotechnology. One-dimensional nanomaterials have gained popularity due to their unique properties and potential applications in several fields such as magnetic memories,[1,2] optoelectronic devices,[2] light-emitting devices, chemical sensors, microresistors, and electrolytic capacitors.[3] It is well known that the properties of nanomaterials are strongly dependent on their size and shape; hence their growth with a good and precise control is one of the crucial requirements for the researchers working in the field of nanoscience and nanotechnology.[4–6] Anodic aluminum oxide (AAO) membrane is widely used in nanotechnology applications and has drawn a great scientific and technological interest in the nanoworld due to its special properties such as high pore density, ideal cylindrical shapes of the pores, controllable pore diameter and periodicity, and a very narrow distribution of pore sizes.[7] These unique properties besides its significant hardness and high thermal and chemical resistance make the AAO membrane suitable for chemical and biochemical separation and also for nanomaterials synthesis[8] comprising nanodots, nanowires[9–11] and nanotubes[10,12,13] of high aspect ratios, and different materials including metals,[1] semiconductors,[14,15] and conducting polymers,[8,16,17] Moreover, an additional advantage with the AAO is that the pore dimensions such as diameter, length, and density can be controlled by varying the process parameters during the anodization.

In order to spread further the applications of AAO membranes a profound knowledge of their physical properties is vital to understand the results and improve the performance of the devices formed thereby. As it is known that various properties of AAO membranes depend on the pore size it is necessary to adjust the pore size.[18–21] The most widely used tool for pore size measurements is scanning electron microscopy (SEM).[1,22] TEM,[23] XRS,[24,25] and AFM[18] also have been used as other methods. Although majority of the methods are destructive and material property dependent, only few are non-destructive. The sample has to be conductive in case of measurement using SEM, and has to be destroyed for TEM measurements.[18] Image analysis has also been used in many cases for estimation of pore size distributions.[24,26,27] Commercially available image processing software suffer few drawbacks such as the uncertainty in the manual delineation made by an expert and small sampling of pore measurements as explained by Raimundo et al.[24] Hence an accurate, efficient, relatively faster, unbiased, and automated method is highly desirable in the nanostructure fabrication process.

In the present work the SEM images of AAO membranes were used for an automated mathematical morphological analysis to obtain quantitative information on pore size distribution. The algorithm used in the method was implemented in MATLAB (The Mathworks, Natick, Massachusetts, USA). The automated measurement of pore size in an SEM image is a

Received 22 June 2011; accepted 3 August 2011.
One of the authors (KSC) gratefully acknowledges Dr. S. Venugopal and Mr. Girish M. of Department of Chemical Engineering, Indian Institute of Science for providing FESEM facility.
Address correspondence to K. S. Choudhari, National Institute of Technology Karnataka, Department of Physics, P. O. Srinivasnagar, Surathkal, Mangalore 575025, India. E-mail: choudhari.k@gmail.com

challenging task due to the variations present in the resolution, contrast, and brightness of the images and hence the identification of the pore itself is non-trivial. While carrying out the pore segmentation the discrepancy caused due to the noise or the calibration errors of the instrument can affect the core segmentation process adversely. Another obstacle in the segmentation process is the foreground-background similarity. The method given by Raimundo et al.[24] used morphological methods to segment the image but the morphological operators may fail when the image is of less contrast, especially in the case of gray-level images, so finding the threshold will be a tough job. Apart from contrast some spurious pores also will enter into the segmented image affecting the pore size detection. In another method proposed by Davidescu et al.,[28] determination of grain size in HVOF MCrAA1Y coatings was carried out by using the number of pixels that constitutes one grain and pore size measurement was based on the area. This method is useful when all the pores are of similar shape and possess close resemblance to the shape of a disk. In this study we propose a technique addressing some of the issues pertaining segmentation and diameter calculation process. Here we make use of Otsu's segmentation method[29,30] to segment the image and calculate the diameter based on the centroid detected by using the morphological operators,[31] hence the diameter measurement is accurate in comparison with the other available methods. This method can calculate diameter even if the pores are not of circular shape. Our approach is capable of addressing most of the problems arising due to the contrast variance and spurious pores intervention. This automated and unbiased algorithm provides a means for accurate measurements of pore properties of the nanoporous anodic aluminum oxides.

EXPERIMENTAL

The experimental procedure comprises the fabrication of AAO membranes, characterization using SEM, and image analysis using mathematical morphology.

Fabrication of AAO

In the fabrication part, before anodization experiments were performed, high-purity aluminum foils (thickness 0.3 mm) were degreased in acetone for 1 h followed by 20 min of ultrasonic cleaning. Then, the samples were annealed at 500°C for 5 h in vacuum. The samples were rinsed with double-distilled water and etched in 2.0 mol/L NaOH at 50°C for 5 min to remove the natural oxide present on the surface. The samples were then dipped in 1.5 mol/L nitric acid for ∼3 min to counteract the remnant lye. After rinsing with double-distilled water again, the specimens were electrochemically polished individually at 200 mA/cm^2 in a mixture of concentrated chromic and phosphoric acids (2:8) for 8 min, rinsed in running double-distilled water and finally dried in the warm air stream. The anodization process was carried out in 0.3 M oxalic acid solution. The temperature of the solution was about 5°C. A two-electrode configuration was used with the electropolished aluminum sample as anode and a cleaned aluminum sheet, of the same area as that of the anode, as cathode. A constant stirring of the electrolyte was maintained throughout the experiments. The duration of the first stage anodization was 2 h. The formed AAO layer was then removed by immersing the specimen in a mixture of 1.8 wt% chromic acid and 6 wt% phosphoric acid at 60°C for 2 h. Subsequent steps of second stage anodization were carried out under the same condition as in the first step, with the 2 h duration. During the first step anodization process, the pores usually nucleate at random positions, and hence the pores on the surface occur randomly and have a broad distribution as can be seen in Figure 1. The substrate, after removing the disordered pore structure using wet chemical etching, appears as shown in Figure 1. However, after the second step of anodization well-ordered and hexagonally arranged pores were obtained (Figure 1). Pore widening is usually performed after the second anodization step using phosphoric acid solution for desired time period and hence required pore dimensions can be achieved. However in this work no pore widening has been performed. After fabrication, samples obtained by the second anodization step were used for SEM and the acquired images were used for pore analysis.

Image Processing and Analysis

The next part of the experimental procedure is to carry out image processing and analysis on the SEM images. The proposed method used in this work mainly concentrates on extracting the pores and calculating the size of the pores based on the centroid point calculated for each pore. The outline of the procedure is discussed subsequently and the detailed explanation is given in the subsequent sections.

1. Find the threshold for segmenting the image into foreground and background. Segment the image based on this threshold value.
2. On the resultant image obtained from step (1) apply the morphological operation-erosion repeatedly with the increasing size of the structuring element (in each iteration) to remove the noises (which will form small pore-like structures) and unnecessary pore connections.
3. The erosion operator might reduce the size of the pores, so apply dilation operator on the image obtained from the step (2) repeatedly with the same structuring elements that are used during erosion. This will provide a regain in the shape without much reduction in the size of the pores.
4. Use the connected component analysis to label all the pores in the image.
5. Calculate the centroid point for each pore using erosion.
6. Calculate the distance of the boundaries from the centroid point for each pore. Here eight different directions will be taken for traversal and the diameters will be calculated.
7. Calculate the average diameter for each pore, from the diameters obtained in step (6). Iterate until all the labeled components are enumerated.

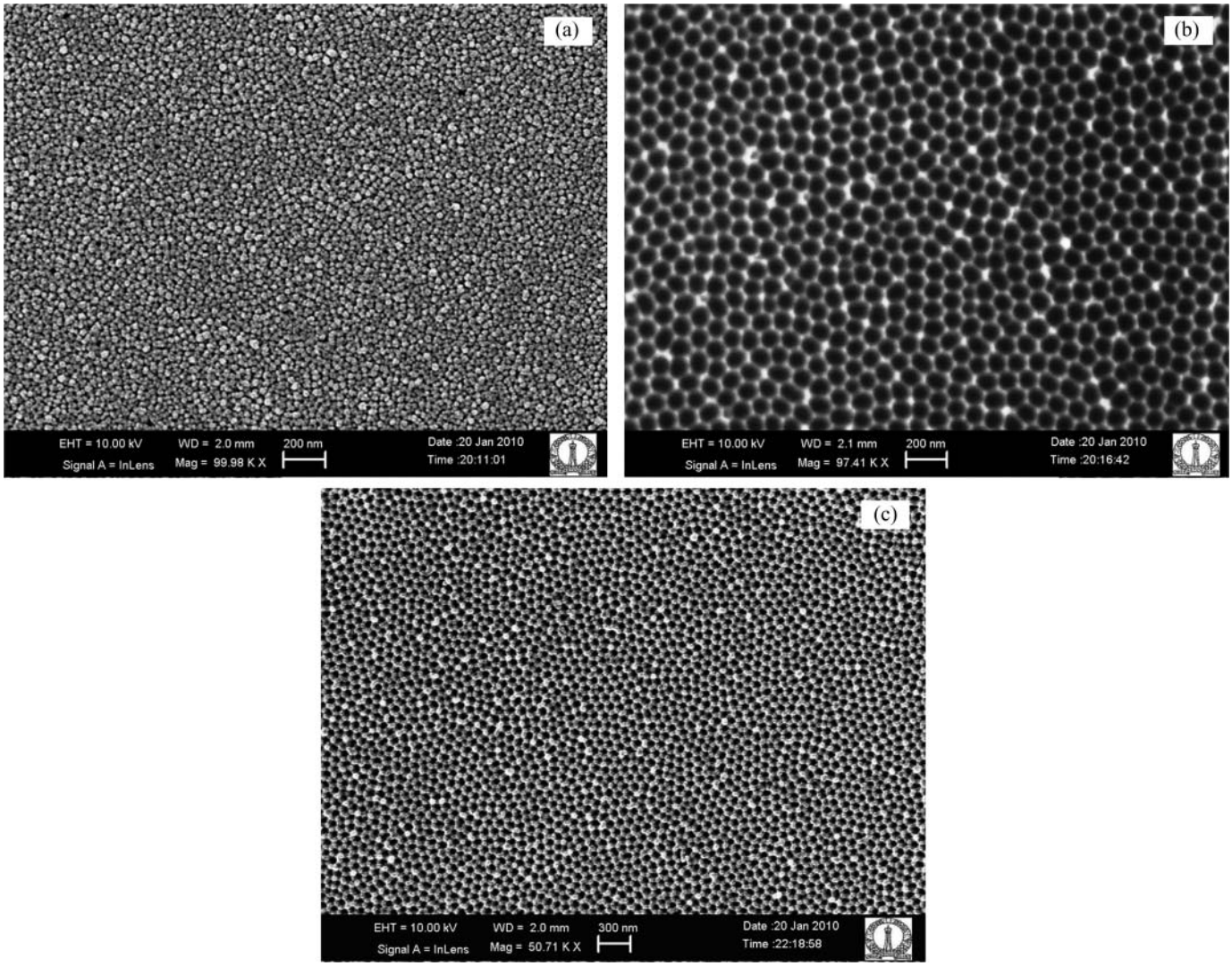

FIG. 1. SEM images of AAO obtained by anodization in 0.3 M oxalic acid, at 40 V, duration 2 h, and at temperature of $\sim 5^{\circ}$C, (a) view of the surface after first-stage anodization, (b) substrate surface after removal of the disordered pore structure, and (c) regular pore structure after second-stage anodization.

Finding the threshold value for segmentation is the major task in this process. The threshold value highly reflects the segmentation process. Here we are using the Advanced Otsu's method[30,32] for finding the threshold. The method is described subsequently:

In this method we are searching for a threshold that minimizes the intraclass variance as defined subsequently:

$$\sigma_w^2(t) = w_1(t) \times \sigma_1^2(t) + w_2(t) \times \sigma_2^2(t) \qquad [1]$$

The weight's w_i s are the probabilities of the two classes separated by the threshold t and σ_i^2 is the variance of the classes. And it can be concluded that the minimization of the intraclass variances is same as maximizing the intraclass variances.[30]

Also,

$$\sigma_b^2(t) = w_1(t) \times w_2(t)\,[\mu_1(t) - \mu_2(t)]^2 \qquad [2]$$

where w_i s are the class probabilities and μ_i s are the class means. The method starts by calculating the probabilities of each intensity level step through all the thresholds from 1 to maximum gray level to find out the maximum value of $\sigma_b^2(t)$ and t corresponding to this value will be the threshold. Then the image is segmented using this threshold (see Figure 2). The threshold image is a binary or bilevel image containing only intensity values 0 and 1. Then the morphological operators are used to remove the unwanted interpore connections and undesired pores detected due to the noises. The morphological operators used here are erosion and dilation, instead of this, an opening (a composite operator consisting of erosion

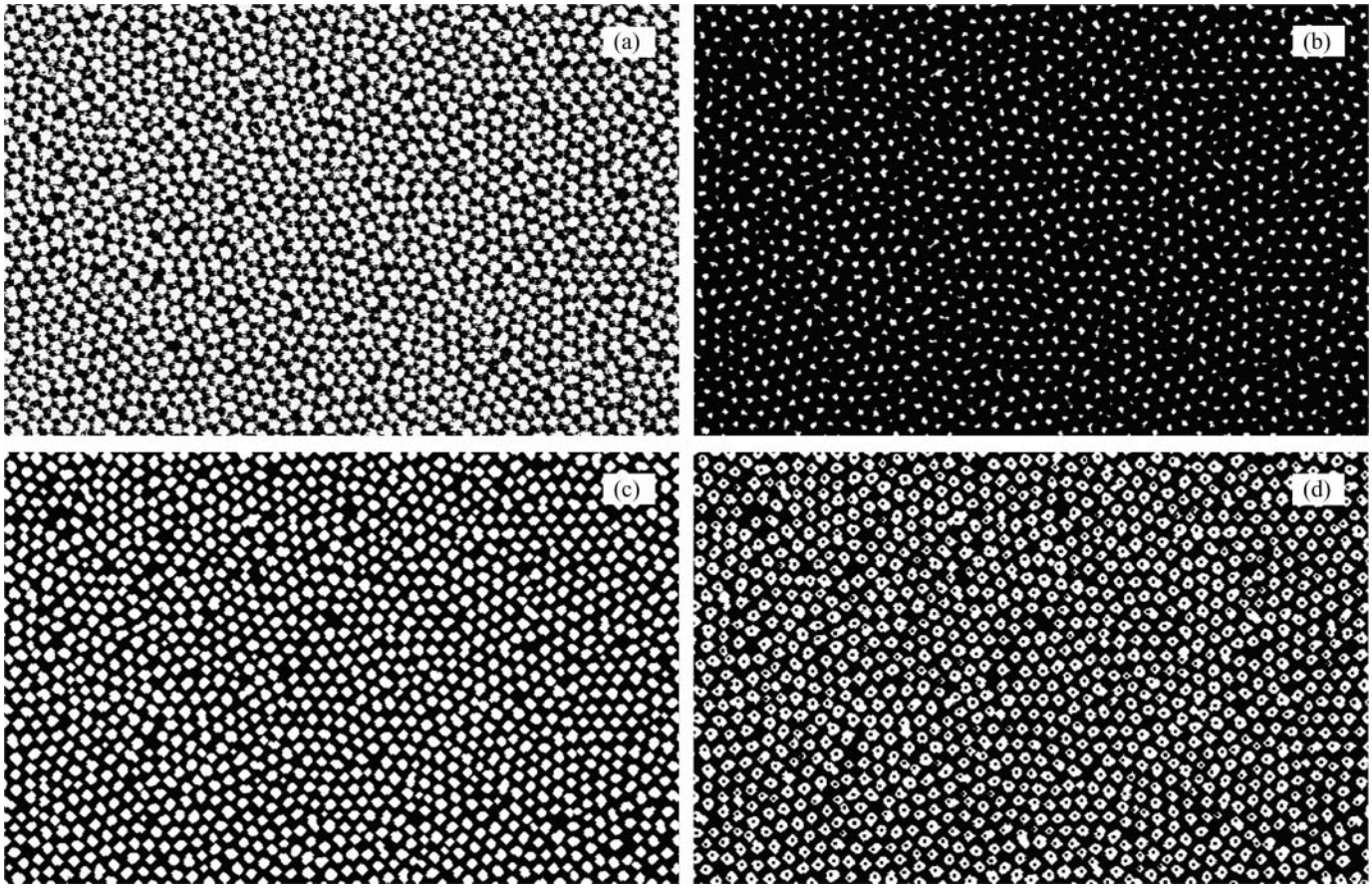

FIG. 2. (a) The segmented image of the original image of Figure 1. (a) A bilevel image, (b) the resultant image after applying repeated erosion to the image of Figure 2(a). (c) The resultant image after applying repeated dilation (the size is regained and the unwanted pores are removed). (d) The centroid points detected are shown in this figure (The size of this image has been slightly increased for the sake of visibility).

and dilation) operator can also be used which can be given as subsequently:

$$O(A, B) = A \circ B = (A \Theta B) \otimes B \quad [3]$$

Here *O(A, B)* stands for opening of *A* with structuring element *B*. The dilation and erosion operations are defined by Eq. 4 and 5, respectively:

$$D(A, B) = A \otimes B = \bigcup_{\beta \in B} (A + \beta) \quad [4]$$

$$E(A, B) = A \Theta (-B) = \bigcap_{\beta \in B} (A - \beta) \quad [5]$$

Here *D(A, B)* is dilation of *A* with structuring element *B* and *E(A, B)* is erosion of *A* with the structuring element *B*. One of the challenging tasks is to deal with small pore-like noises that contribute toward the calculation of the pore sizes. These noises are to be removed without affecting the existing pore structures; we use erosion and dilation repeatedly to remove these unwanted pore-like noises.[28] First, we use erosion repeatedly with structural elements of different sizes (disks with varying diameters are used) such that the size of the structuring element is increased in each iteration so as to remove majority of these noise components. But erosion will reduce the size of the pores as well. For addressing this problem we carry out dilation repeatedly with the same kind of structural elements that were used for erosion (in the same size sequence). This will regain the size. Figure 2 shows the results using repeated erosion and dilation. So these repeated operations will result in the image formation with less noise and removal of all the unwanted pore connections, which would adversely affect the image-labeling process.

RESULTS AND DISCUSSION

The image of Figure 1 was supplied as an input image. The threshold was obtained as 74 and the image was segmented with this value. All the background pixels were made as dark and the foreground ones (pores) were made white. The resulting image is shown in Figure 2. In this figure the protuberances are visible in the boundaries of the pores and some undesired connections among pores are also evident, so we remove all

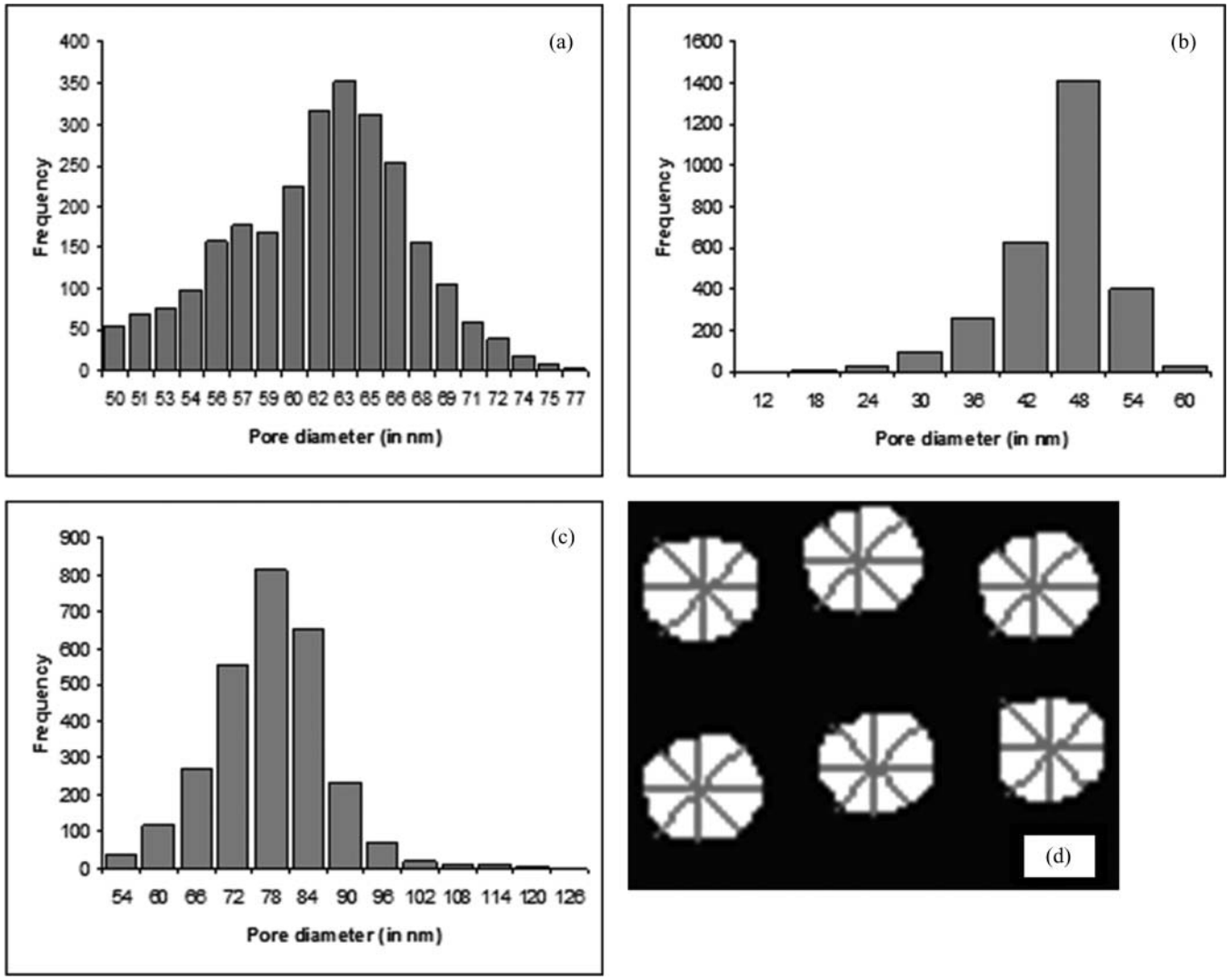

FIG. 3. The histograms showing (a) average, (b) small, and (c) large diameter distributions. (d) Image showing the pore traversal in four different directions to find the average diameter of the pores (only few pores are shown in an enlarged view).

these discrepancies using the repeated dilation and erosion with the structuring element of varying sizes. In this work we used disk as the structuring element and the size of the disk was varied from 1 to 3, the upper limit was detected dynamically. The results obtained after applying erosion and dilation are shown in Figure 2. Here we can see that all unwanted pore-like structures (noises) and unwanted pore connections are eliminated. The resultant image was taken through a labeling process in which all the components were labeled. In this particular case there were 500–600 labeled components, which were used to separate out the pores.

The next step was to determine the centroid of the pores; this was done using erosion. Erosion with the structuring element (disk) of different sizes was applied on each of the pores obtained after the labeling process, and the image just before getting fully blacked out gave the centroid of the pores. From this centroid information the sizes of the pores were calculated based on the traversal procedure explained, as follows.

In the traversal procedure we adopted a method to traverse from the centroid to the edge of the pores in different directions—horizontal, vertical, and diagonal (along both the diagonals). The algorithm traverses in these directions until the edge of the pore or image is reached. Here we get four different diameters, one along horizontal direction, one along vertical, and one each along two diagonals and the average diameter values are obtained from these. The pore traversal is shown in Figure 3. The spread in the small and large pore distribution highlights the center point detection as well as the shape of the pores. If the pores are close to the shape of a circle then the spread in the distributions will be very less. On the other hand, if the pores are of irregular shapes or the segmentation was not able to segment the pores properly then the spread will be

more pronounced in the distributions. If the spread exceeds the threshold then the quality of the image will have poor contrast and the noises will not have been eliminated fully in the image. Thus the images are to be preprocessed before segmentation.

The large pore distribution indicates the number of pores that are joined together in the segmented image, and the small pore distribution quantifies the number of false pores that are contributing toward the diameter detection process. In Figure 3 it can be seen that the majority of the small pores are concentrated toward the size range of 40–60 nm, so very less spurious pores are identified to be contributing toward the diameter detection process. And in case of large pore distribution majority of the pores are also within the range of 50–80 nm and fewer pores are joined together to form a single pore during the segmentation process. Most of the pores are observed to have the average diameter in the range of 60–70 nm. These values are in agreement with the data obtained by manual diameter measurements performed on SEM images. Hence these pore size distribution results obtained from the mathematical morphological analysis carried out on the SEM images of the porous alumina structures, as demonstrated previously, serves as a valuable tool in the field of nanomaterial research helping in efficient, accurate, automated, and unbiased control of the process parameters of the nanomaterial fabrication procedure.

The presented algorithm can be used on the images with any pore sizes. There is no constraint on the pore sizes as far as the algorithm is concerned. The case of nanoporous alumina prepared in 0.3 M oxalic acid, used here, is for illustration purpose only. Generally, any SEM/FESEM image with reasonably good contrast can be comfortably dealt with using the present algorithm. In case of noisy figures with somewhat low contrast the denoising (pre-processing) step can handle the situation without much intricacy. However, if the pores in the image are very small and the size of the pores is comparable to few pixels then the chance of counting any artifact in the image of such small size range as pores would be slightly higher. But this would be a rare case as a typical SEM/FESEM image would usually have significant clarity and contrast rendering the algorithm work efficiently without any problem. The algorithm can handle images with any magnification without any specific limit on the lower value of the magnification. It would a good idea to use the images with the lower magnification SEM images for the analysis as large areas of the sample surface can be accommodated giving better results on the pore-size distribution provided the pores in the image are free from indistinctness. Also magnifying the pores beyond a limit can weaken the edges present in the images and this may affect the proper threshold selection for segmentation of the pores. Considering these two facts which are not serious limitations though, a proper analysis can be carried out without any difficulty.

CONCLUSION

AAO nanostructures have been prepared by a two-step anodization process. In this work a new method has been introduced based on morphological operators for the determination of the pore size distributions of AAO. The method utilizes the concept of finding the centroid of each pore used for calculation of pore diameters. The method is also capable of handling the discrepancies caused due to the noisy data, which usually form false pores in the threshold image during analysis. The presented procedure has been tested with the SEM images of various samples with different magnification, resolution, and pore sizes of AAO; it has provided good estimate of the quantitative data on pore diameter in all the cases. The method that we have presented here can be used with little or no modification in the algorithm for various nanostructure dimension determination and quantitative data acquisition tasks enabling an efficient, unbiased, and reliable control of the process parameters in the fabrication process of nanostructures.

REFERENCES

1. Masuda, H.; Fukuda, K. Ordered metal nanohole arrays made by a two-step replication of honeycomb structures of anodic alumina. *Science* **1995**, *268*, 1466–1468.
2. Zhou, J.; He, J.; Zhao, G.; Zhang, C.; Zhao, J.; Hu, H. Alumina nanostructures prepared by two-step anodization process. *Trans. Nonferrous Met. Soc. China* **2007**, *17*, 82–86.
3. Mozalev, A.; Mozaleva, I.; Sakairi, M.; Takahashi, H. Anodic film growth on Al layers and Ta-Al metal bilayers in citric acid electrolytes. *Electrochim. Acta.* **2005**, *50*, 5065–5075.
4. Hu, M.; Chen, J.; Li, Z.; Au, L.; Hartland, G.V.; Li, X.; Marquez, M.; Xia, Y. Gold nanostructures: Engineering their plasmonic properties for biomedical applications. *Chem. Soc. Rev.* **2006**, *35*, 1084–1094.
5. Eustis, S.; Sayed, M.A. E. Why gold nanoparticles are more precious than pretty gold: Noble metal surface plasmon resonance and its enhancement of the radiative and nonradiative properties of nanocrystals of different shapes. *Chem. Soc. Rev.* **2006**, *35*, 209–217.
6. Li, X.; Wang, D.; Tang, L.; Dong, K.; Wu, Y. Controllable synthesis of Ag nanorods using a porous anodic aluminum oxide template. *Appl. Surf. Sci.* **2009**, *255*, 7529–7531.
7. Thongmee, S.; Pang, H.L.; Ding, J.; Lin, J.Y. Fabrication and magnetic properties of metallic nanowires via AAO templates. *J. Magn. Magn. Mater.* **2009**, *321*, 2712–2716.
8. Ren, Y.; Zhang, K. How structure changes in fabrication of large size ordered anodic alumina film? *Mater. Lett.* **2009**, *63*, 1925–1927.
9. Sauer, G.; Brehm, G.; Schneider, S.; Neilsch, K.; Wehrspohn, R.B.; Choi, J.; Hofmeister, H.; Gosele, U. Highly ordered monocrystalline silver nanowire arrays. *J. Appl. Phys.* **2002**, *91*, 3243–3247.
10. Marsal, L.F.; Vojkuvka, L.; Formentin, P.; Pallares, J.; Borrull, J.F. Fabrication and optical characterization of nanoporous alumina films annealed at different temperatures. *Opt. Mater.* **2009**, *31*, 860–864.
11. Zhang, Z.; Gekhtman, D.; Dresselhaus, M.S.; Ying, J.Y. Processing and Characterization of single-crystalline ultrafine bismuth nanowires. *Chem. Mater.* **1999**, *11*, 1659–1665.
12. Steinhart, M.; Wendorff, J.H.; Greiner, A.; Wehrspohn, R.B.; Neilsch, K.; Schilling, J.; Choi, J.; Gosele, U. Polymer nanotubes by wetting of ordered porous templates. *Science* **2002**, *296*, 1997.
13. Xiao, Z.L.; Han, C.Y.; Welp, U.; Wang, H.H.; Kwok, W.K.; Willing, G.A.; Hiller, J.M.; Cook, R.E.; Miller, D.J.; Crabtree, G.W. Fabrication of alumina nanotubes and nanowires by etching porous alumina membranes. *Nano Lett.* **2002**, *2*, 1293–1297.
14. Sander, M.S.; Gronsky, R.; Sands, T.; Stacy, A.M. Structure of bismuth telluride nanowire arrays fabricated by electrodeposition into porous anodic alumina templates. *Chem. Mater.* **2003**, *15*, 335–339.

15. Miao, Z.; Xu, D.S.; Ouyang, J.H.; Guo, G.; Zhao, X.; Tang, Y. Electrochemically induced sol-gel preparation of single-crystalline TiO 2 nanowires. *Nano Lett.* **2002**, *2*, 717–720.
16. Belwalkar, A.; Grasing, E.; Geertryuden, W.V.; Huang, Z.; Misiolek, W.Z. Effect of processing parameters on pore structure and thickness of anodic aluminum oxide (AAO) tubular membranes. *J. Membr. Sci.* **2008**, *319*, 192–198.
17. Wang, C.W.; Wang, Z.; Li, M.K.; Li, H.L. Well-aligned polyaniline nanofibril array membrane and its field emission property. *Chem. Phys. Lett.* **2001**, *341*, 431–434.
18. Choi, D.H.; Lee, P.S.; Hwang, W.; Lee, K.H.; Park, H.C. Measurement of the pore sizes of anodic aluminum oxide (AAO). *Curr. Appl. Phys.* **2006**, *6S1*, e125–e129.
19. Horowitz, G.; Fichou, D.; Peng, X.; Garnier, F. Thin-film transistors based on alpha-conjugated oligomers. *Synthetic Met.* **1991**, *41–43*, 1127–1130.
20. Nelson, S.F.; Lin, Y.Y.; Gundlach, D.J.; Jackson, T.N. Temperature-independent transport in high-mobility pentacene transistors. *Appl. Phys. Lett.* **1998**, *72*, 1854–1856.
21. Whitney, T.M.; Searson, P.C.; Jiang, J.S.; Chien, C.L. Fabrication and magnetic properties of arrays of metallic nanowires. *Science* **1993**, *261*, 1316–1319.
22. Li, A.P.; Muller, F.; Birner, A.; Nielsch, K.; Gosele, U. Polycrystalline nanopore arrays with hexagonal ordering on aluminum. *J. Vac. Sci. Technol. A.* **1999**, *17*, 1428–1431.
23. Nielsch, K.; Choi, J.; Schwirn, K.; Wehrspohn, R.B.; Gosele, U. Self-ordering regimes of porous alumina: The 10% porosity rule. *Nano Lett.* **2002**, *2*, 677–680.
24. Raimundo, D.S.; Caliopre, P.B.; Huanca, D.R.; Salcedo, W.J. Anodic porous alumina structural characteristics study based on SEM image processing and analysis. *Microelectr. J.* **2009**, *40*, 844–847.
25. Campbell, L.; Kemmitt, T.; Bowden, M.; Kirchner, A. Growth of AlPO4–5 within the pores of anodic alumina. *Curr. Appl. Phys.* **2008**, *8*, 479–481.
26. Kohel, L.; Zeng, X. Digital image analysis to determine pore size distribution of nonwoven fabrics. *IMACS Multiconf. Comput. Eng. Sys. Appl.* **2006**, 145–149.
27. Dimassi, M.; Koehl, L.; Zeng, X. Modeling of the pore network by image processing: Application to the nonwoven material. *IMACS Multiconf. Comput. Eng. Sys. Appl.* 171–177.
28. Davidescu, A.; Savii, G.G.; Sticlaru, C.J. Analysis of HVOF-SPRAYED MCrAlY coatings using SEM image processing. *Optoelectron. Adv. M.* **2005**, *7*, 3107–3110.
29. Jain, A.K. *Fundamentals of Digital Image Processing*; Prentice Hall: Englewood Cliffs, NJ, 2002.
30. Otsu, N.A threshold selection method from gray-level histograms. *IEEE T. Syst. Man.* **1979**, *SMC9*, 62–66.
31. Gonzales, R.; Woods, R.E. *Digital Image Processing*; Pearson Education: New York, 2002.
32. Liao, P.S.; Chen, T.S.; Chung, P.C.A fast algorithm for multilevel thresholding. *J. Inf. Sci. Eng.* **2001**, *17*, 713–727.